Use of the Variable Gain Settings on SPOT

Pat S. Chavez, Jr.
U. S. Geological Survey, 2255 North Gemini Drive, Flagstaff, AZ 86001

ABSTRACT: Often the brightness or digital number (DN) range of satellite image data is less than optimal and uses only a portion of the available values (0 to 255) because the range of reflectance values is small. Except for SPOT (Systeme Probatoire d'Observation de la Terre), most imaging systems have been designed with only two gain settings, normal and high. The SPOT High Resolution Visible (HRV) imaging system has the capability to collect image data using one of eight different gain settings. With the proper procedure this allows the brightness or reflectance resolution, which is directly related to the range of DN values recorded, to be optimized for any given site as compared to using a single set of gain settings everywhere.

The island of Hawaii was used as the test site and normal/standard (5,6,5) and high/maximum (8,8,8) gain SPOT images were collected simultaneously using the HRV1 and HRV2 imaging systems, respectively. Old Landsat MSS (multispectral scanner) data were used to predict in advance the optimum SPOT gain settings for the given site. The high gain data showed detail through DN changes that are equivalent to less than half a DN of the normal settings and could not be shown in the normal gain data. The results indicate that the normal/standard gain settings currently being used may be too low for many areas.

INTRODUCTION

THE USE OF DIGITAL IMAGES recorded by imaging systems onboard orbiting satellites is becoming more widespread. Digital image data have been widely available since 1972 when the first Landsat satellite carrying the multispectral scanner (MSS) imaging system was launched. In addition to the MSS system, the Landsat satellites launched in 1982 and 1984 carried the Thematic Mapper (TM) imaging system. The TM data have improved spatial and spectral resolution as compared to the MSS data. The MSS data have approximately 79 metre by 79 metre spatial resolution and four spectral bands; the TM data have approximately 30 metre by 30 metre spatial resolution and six spectral bands, plus a 120 metre by 120 metre resolution thermal band.

With the launching of SPOT (Systeme Probatoire d'Observation de la Terre) in early 1986, the desimination of digital image data collected from space and available to the general public became an international enterprise. SPOT data have improved spatial resolution as compared to the Landsat TM data (three 20 metre by 20 metre multispectral bands and a 10 metre by 10 metre panchromatic band).

With the need to collect image data from all parts of the Earth's surface, imaging systems must be designed to image scenes that contain targets with both dark and bright albedo surfaces. For example, forested and water-covered areas have dark albedos while deserts and snow-covered areas have bright albedos. Usually, because of this requirement, the actual digital number (DN) range of images collected from satellites is less than optimal, filling only a portion of the available range of 0 to 255 on Landsat TM and SPOT. Except for SPOT, most imaging systems have been designed with only two gain settings, normal and high. The gain settings allow the brightness or reflectance resolution to be increased or decreased, affecting the DN range within an image. The high-gain settings on Landsat have not readily been available in an operational sense and are available only upon special request. Generally, the standard gain settings are used when collecting data of areas with both dark and bright albedos. This means that the gain and offset values used to convert radiance values in analog form to digital numbers are constant for a given band on a given satellite, regardless of the target being imaged or the application.

The SPOT imaging system has the capability to collect digital image data using one of eight different gain settings. Three are higher than normal and four are lower than normal (Courtois, 1984). With the proper selection, the brightness or reflectance resolution for any site, which is directly related to the range of DN values, can be optimized.

The gain settings required to optimize the brightness or reflectance range of a particular area within the available DN range will be influenced by (1) the range of the reflectance values for each spectral band within the area of interest, (2) the sun elevation, (3) atmospheric conditions, and (4) the topography. The objective in this paper is to show the results of the use of the variable gain settings of SPOT. The optimal gain settings for the given test site were predicted using Landsat MSS data and an intersensor calibration technique developed by the author. This calibration procedure is the subject of another paper and is outside the scope of this paper.

TEST SITE AND DATA CHARACTERISTICS

The large island of Hawaii was used as the test site due to the generally dark reflectance of the various cover types in the area (volcanic rocks, dense vegetation, and ocean water). A low reflectance site was chosen to test the variable gain capability in case the predicted results were not as expected. A dark test site would allow for possible errors without saturating to a DN value of 255. However, there were areas with high reflectance values in the image. The center of the image is just to the right of the Mauna Loa volcano and includes both barren dark volcanic rocks and highly-to sparsely-vegetated areas. About 5-7 percent of the pixels within the SPOT image used in this project are ocean water and approximately 43 percent are clouds.

The SPOT 20-metre multispectral (XS) data were collected on 27 June 1987. The world reference scene number is K473, J311. SPOT XS data with both the normal (5,6,5) and maximum/high (8,8,8) gain settings were collected simultaneously using the HRV1 and HRV2 (High Resolution Visible) imaging systems, respectively. The sun elevation during data collection was 67.8 degrees with an azimuth of 75.7 degrees. The digital data delivered were in level 1A format (i.e., radiometric correction but no geometric resampling).

The Landsat MSS data used to compute the optimal SPOT gain settings were collected on 11 February 1973. The Landsat path and row numbers are 67 and 46, respectively; the scene ID is 1203-2018000. The normal gain settings were used. The sun elevation during data collection was 41.0 degrees with an azimuth of 132.0 degrees.

GAIN SETTING CALCULATIONS

The Landsat MSS data were used to compute the approximate minimum, average, and maximum reflectance values within each

PHOTOGRAMMETRIC ENGINEERING AND REMOTE SENSING,
Vol. 55, No. 2, February, 1989, pp. 195–201.

0099-1112/89/5502–195$02.25/0

spectral band for the area of interest. This was done in order to estimate/predict the optimal SPOT gain settings for the same area. These reflectance values were computed by first removing the effects of the gain and offset values used by Landsat (i.e., converted from DN to radiance). The data were then corrected for first-order atmospheric scattering and sun elevation effects (Chavez, 1988). These computed reflectance values were then adjusted to the sun elevation of the SPOT data, and a first-order atmospheric scattering effect was added to estimate the range of SPOT radiances. Finally, the various SPOT gain settings were applied to these new radiance values to predict the equivalent SPOT DN values. This approximating procedure was used to identify the highest gain settings that could be used on the SPOT XS bands without saturating the maximum reflectance of interest to a DN value of 255.

The SPOT imaging system has eight different gain settings available; the ratio of any two consecutive gain settings is equal to 1.3 (Begni *et al.*, 1985). The value of a particular gain is computed as follows:

$$\text{GAIN} = 1.3^{(M-3)};\ M = 1,8 \qquad (1)$$

Notice that for $M = 3$ the gain value of 1.0 is used, which translated to no gain except for the absolute calibration values. The normal/standard gain settings for SPOT are M equals five for bands XS1 and XS3 and M equals six for band XS2 (Begni *et al.*, 1985). The advantage of using the highest possible gain settings is that the ability to record incremental differences in reflectance levels is improved. The dynamic range improvement is not limited to only dark areas; the incremental DN difference between the normal- and high-gain images can be seen at all brightness levels.

For the Hawaii test site, the maximum settings available were identified as the optimum ones to use. In fact, the computed results indicated that higher gain settings could have been used for XS1 and XS2 without saturation in the area of maximum reflectance. The original test reflectance targets did not include clouds; however, interesting results were seen in the final SPOT data which had about 43 percent clouds.

Subareas representing dark, midtone, and bright regions were used to statistically and visually compare and evaluate the difference between the normal- and high-gain images. The image products used in the analysis included (1) the original, (2) high-pass filtered (HPF), and (3) vertical first difference images. The variance and percentages at midrange of these images were compared. For visual analysis, the data had hard linear contrast stretches applied before generating prints.

As a side note, as of mid-1988 the availability of the variable gain option to the general user community was not clear. Apparently the user cannot request gain settings of his/her choice. Gain settings of low, medium, or high can be requested but CNES will decide what this means for the given area (Rob Lees, personal commun., April 1988). The maximum gain settings ($M = 8$) cannot be requested by the user because the noise level could be unacceptable (Rob Lees, personal commun., April 1988). However, in this project the normal gain settings data had more noise/striping than did the high/maximum gain settings data. This could be due to the fact that with the maximum gain settings the detector-to-detector radiometric calibration actually works better because of the improved radiance resolution (i.e., one-half DN versus one DN incremental difference in the image data).

RESULTS AND DISCUSSION

The high/maximum gain setting images show brightness detail that would be the equivalent of less than half a DN change in the normal/standard gain setting images. The differences between the normal ($M = 5,6,5$) and high ($M = 8,8,8$) gains are approximately 2.2 for bands XS1 and XS3 and 1.7 for band XS2. It is interesting to note that the number of pixels saturated to a DN value of 255 in the high-gain data for XS1, XS2, and XS3 were 33.9, 25.9, and 30.0 percent, respectively. This compared to 14.1, 5.6, and 0.8 percent for the normal-gain data. Because there is approximately 43 percent cloud cover, determined by saturating the cloud pixels to 255 with an interactive stretch program and identifying the DN location in the image histogram, even in the high-gain mode all the clouds were not saturated.

Statistical Comparison

Both the HPF and first-difference algorithms are designed to enhance local detail and are affected by the amount of DN changes within the neighborhood of the filter (Chavez *et al.*, 1976; Chavez and Bauer, 1982; Chavez and Berlin, 1984). The less local the detail, the more homogeneous the DN values are within a given area/window, and the more pixels that are assigned to or near the midrange, indicating no difference between a pixel and its surrounding neighborhood. The HPF centers the output DN values at 127.5 (127 and 128) and the first difference at 127.

Shown in Table 1 for both the normal- and high-gain three SPOT XS bands are the standard deviation and midrange percentage of the original image, 11 by 11 HPF, 21 by 21 HPF, and vertical first-difference image for the dark subarea (Mauna Loa volcano). The percentage of pixels with DN values at midrange are shown because these values are an indication of the amount of subtle changes present in the image (Chavez and Bauer, 1982). For example, in a vertical first-difference image if 60 percent of the pixels are at midrange (DN value of 127), which indicates no difference, the amount of local detail is less than in a first-difference image that contains only 30 percent of its pixels at midrange. The differences in the standard deviations of the normal- versus high-gain images are approximately the same ratios seen between the gain values used, as is expected. The standard deviation of the HPF images of the high-gain data are increased as compared to the HPF images of the normal-gain by about 10 and 20 percent for the 11 by 11 and 21 by 21 HPFs, respectively. The increase for the first-difference images is about 10 percent.

Table 1 also shows that there is a dramatic decrease in the number of pixels at or near the midrange DN values for the HPF and first-difference high-gain images as compared to the normal-gain images. There are from 44 to 125 percent more pixels at midrange in the normal- versus the high-gain images, with the overall average difference in the number of pixels at midrange equal to 70 percent. XS1 had the largest differences between the number of pixels at midrange, but it also had more noise (vertical striping) than the other two bands. However, for bands XS2 and XS3 for all three image products, the difference in the number of pixels at midrange is still high (57 percent). The vertical first-difference image, which does not see the vertical striping, has a difference of 85 percent for XS1.

Visual Comparison

In order to visually compare and evaluate the two data sets, the user must be aware of what doubling the gain will do to the data. If color composites and/or black-and-white prints are made using standard linear contrast stretches on both the normal- and high-gain images, little, if any, difference will be visually detectable at typical image scales used for photointerpretation (see Figures 1a and 1b). This is because the changes that occur are at the one to one-half DN level, and the overall contrast of the entire image, overshadows the subtle local changes.

In order to see local detail where the level of DN differences is small, either very hard contrast stretches must be applied to a selected narrow DN range (Figures 1c and 1d) or spatial filtering techniques that enhance local detail must be used (Chavez and

TABLE 1. STANDARD DEVIATION AND MIDRANGE PERCENTAGES FOR THREE NORMAL- AND HIGH-GAIN SPOT XS BANDS, MAUNA LOA, HAWAII. THE INFORMATION SHOWN IS FOR THE ORIGINAL, 11 BY 11 HIGH PASS FILTER (HPF), 21 BY 21 HPF, AND FIRST DIFFERENCE IMAGES.

IMAGE	ORG SD	11 × 11 SD	21 × 21 SD	1st DIFF SD	MID RNG% 11 × 11	MID RNG% 21 × 21	MID RNG% 1st DIFF
Normal XS1	5.0	6.3	6.3	6.0	63.7	52.3	57.2
Normal XS2	7.8	6.4	6.5	6.1	60.3	49.7	55.2
Normal XS3	6.9	6.3	6.3	6.0	66.3	55.4	61.9
High XS1	11.5	7.1	7.7	6.5	28.2	29.0	31.0
High XS2	14.7	7.0	7.7	6.4	41.8	32.5	34.7
High XS3	15.8	7.0	7.6	6.4	43.5	32.8	37.9

Berlin, 1984). In the following examples these types of image processing algorithms were used to show the difference between the normal- and high-gain images. Both color composites and black-and-white prints of the enhanced results were used in the analysis; however, only black-and-white prints are shown due to cost and space limitations. The results were similar in the three bands, as is shown by the statistics in Table 1. As stated earlier, XS1 of the normal data set did have more vertical striping than the high-gain XS1 image, but visually the results were similar to those seen in XS2 and XS3. The differences between the normal- and high-gain images are easier to see if the image products are viewed at larger scales than those typically used for photointerpretation. This can be done by either using an 8× loupe or digitally enlarging the images to allow prints to be made at larger scales than usual. The images shown here have been through a 7× digital enlargement and were then smoothed with a 7 by 7 filter to reduce the "blocky" appearance introduced by the digital enlargement (Chavez *et al.*, 1984).

The visual differences seen between the normal- and high-gain data are directly related to the contouring versus noncontouring effects caused by compressing the brightness or DN range in one image relative to the other. For example, if a range of ten DN are compressed to a new range of four or five DN, which is the approximate difference between the high- and normal-gain data, quantizing or contouring effects will be seen in the compressed image at the local scale. This effect will be especially noticeable on image products generated using algorithms designed to enhance local detail, such as with high-pass filtering and first-difference algorithms. The set of images shown in Figures 1 to 4 are products of the Mauna Loa volcano area. The inside of the crater has very dark volcanic rocks while the outside slopes have basalts that are not as dark and vegetation. Figure 5 shows an example of an area with much higher reflectance values that the Mauna Loa area.

As stated earlier, Figures 1a and 1b show the normal- and high-gain original XS2 images with standard linear contrast stretches and Figures 1c and 1d with very hard linear contrast stretches applied to enhance the dark areas. Some of the local detail present only in the high-gain image can be seen in the hard-stretched products. However, the local detail differences and the quantizing/contouring can be seen better in the high-pass filtered images. Figures 2a and 2b show the results of the 11 by 11 HPF, and Figures 3a and 3b show the results of the 21 by 21 HPF. Notice that, due to the quantizing effects, the fissure going through the center of the crater can be seen better in the high-gain image. This results from the increased incremental DN difference or reflectance/radiance resolution in the high-gain data and not in the normal-gain data. The high-gain data have approximately twice as fine a brightness resolution due to the gain difference, so it can show the subtle contrast between the fissure and the surrounding background. Keep in mind that similar results are also seen in areas with bright reflectance.

Figures 4a and 4b are image results of the vertical first difference, which approximates the vertical first derivative, of the normal- and high-gain images. The vertical direction was selected in order to minimize the vertical striping effects on the results. The algorithm looks at DN differences that occur at the pixel level (Chavez and Bauer, 1982). Notice that the normal-gain image (Figure 4a) has more pixels at midtone, which implies no difference, as compared to the high-gain image (Figure 4b). This agrees with the statistics shown in Table 1, which indicate 55.2 percent at no difference for the normal XS2 image versus 34.7 percent for the high-gain XS2 image. This implies that the normal-gain image is less busy or more homogeneous at the local level than is the high-gain image, as expected.

Figures 5a and 5b show an example of an area which has much higher reflectance than does the dark Mauna Loa volcano area. The DN values of this subarea is in the middle to upper portion of the entire XS3 image histogram. Shown are the 11 by 11 high-pass filtered results for both the normal- and high-gain XS3 images. As can be seen, the results in this area are similar to those in the dark Mauna Loa area. The difference in the gain between the XS3 images is 2.2 as compared to 1.7 for the XS2 images. This makes the quantizing/contouring in the normal data more severe as compared to the high-gain data.

As mentioned earlier, even in the high-gain images all the clouds did not saturate and the maximum noncloud reflectances in SPOT bands XS1 and XS2 were not close to saturation. In the near-infrared XS3 band the DN values of the maximum noncloud reflectance were near 240. The pixels with these high DN values were occuring in densely vegetated areas that typically have a high infrared response during this time of the year.

CONCLUSIONS AND RECOMMENDATIONS

Because all the clouds did not saturate and their reflectance is relatively high in comparison to most other cover types, the results indicate that the high/maximum gain settings of SPOT can be used in many areas without causing a saturation problem. This would allow digital images to be collected with the maximum possible DN range and reflectance resolution, improving the discrimination capability of the image data. Extensive testing should be performed to determine what conditions would cause saturation problems. Perhaps problems would be encountered only over bright deserts during high sun elevation; the snow-covered areas near the poles benefit from the low sun elevation that usually exists in these regions.

Based on the results of this project, if the maximum gain settings are used over dark mountainous terrain, the local detail should be improved. There are several applications that could benefit from this improvement. For example, applications that use digital image correlation, such as image-to-image control-point identification and digital correlation for automatic stereo compilation, would benefit. Also, applications that make use of spatial filtering algorithms could benefit because of the increased local detail that would be present in the image.

The variable gain of SPOT is a new capability that has not existed in previous systems. It was advertised as a new improved capability (Courtois, 1984). However, because of the

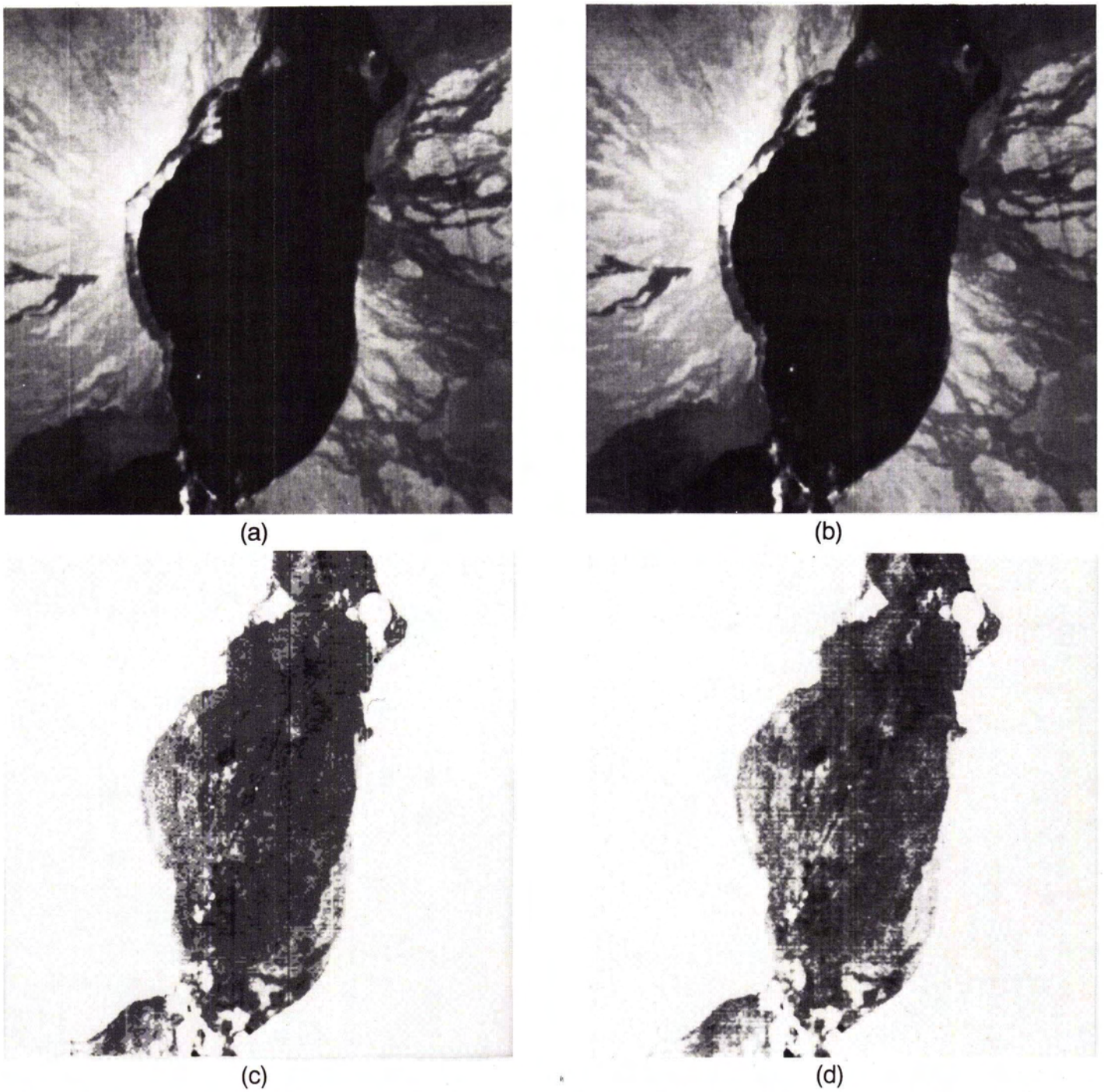

FIG. 1. (a) and (b) show the normal- and high-gain original XS2 data, respectively. The area is centered on the Mauna Loa volcano on the big island of Hawaii. The inside of the crater has very dark volcanic rocks while the outside slopes have both basalts, which are not as dark, and vegetation. Standard type linear contrast stretches were applied to both images. The same percentage of saturation from 0 to 255 DN was used to keep the overall contrast of both images the same. North is approximately at the top and the distance top-to-bottom of the crater is about 6 km. Note that with standard type linear contrast stretches it is difficult to see any difference because the overall contrast overshadows the small local DN changes. (c) and (d) show the normal- and high-gain original XS2 data with very hard linear contrast stretches, respectively. The data were stretched to enhance the dark/lower region of the histogram and show detail within the crater. Note that some of the quantizing/contouring effects can be seen in the normal-gain image; however, the high-pass filtered prints in Figures 2 and 3 show this effect more dramatically. SPOT image Copyright 1987 CNES.

limited access to this capability, this has put SPOT close to the same category as the other systems that collect data with the same constant settings regardless of the type of area being imaged or the intended application of the data. The results obtained in this project indicate that perhaps the decision to not make the variable gain option available to the users other than in the low, medium, or high type mode should be reviewed. At a minimum, the normal gain settings should be reviewed and changed to higher settings if further testing indicates that a saturation problem will not occur, perhaps something like

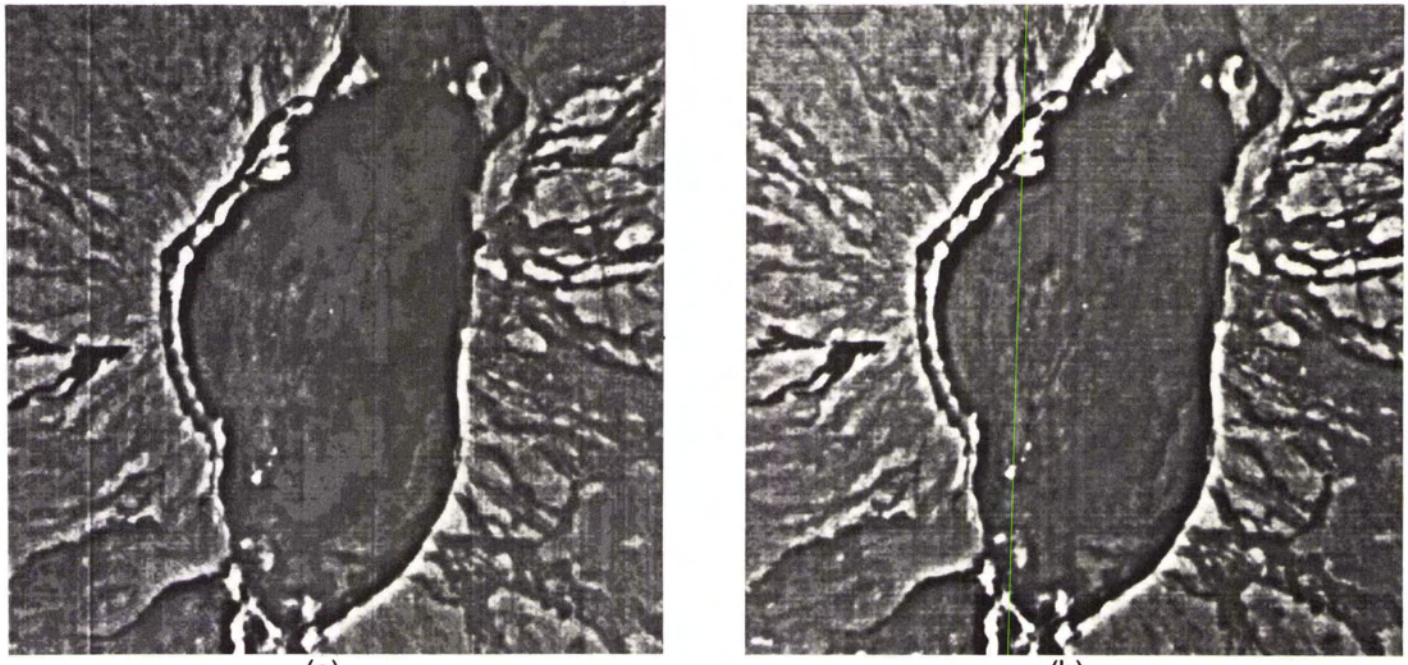

FIG. 2. (a) and (b) show the results of applying an 11 by 11 high-pass filter (HPF) to the normal- and high-gain XS2 images, respectively. The quantizing/contouring effects due to the smaller compressed DN range of the normal gain image (1.7 difference) can easily be seen, especially inside the Mauna Loa crater where the variation in reflectance is small. The HPF results had hard linear contrast stretches applied for visual analysis and display. SPOT image Copyright 1987 CNES.

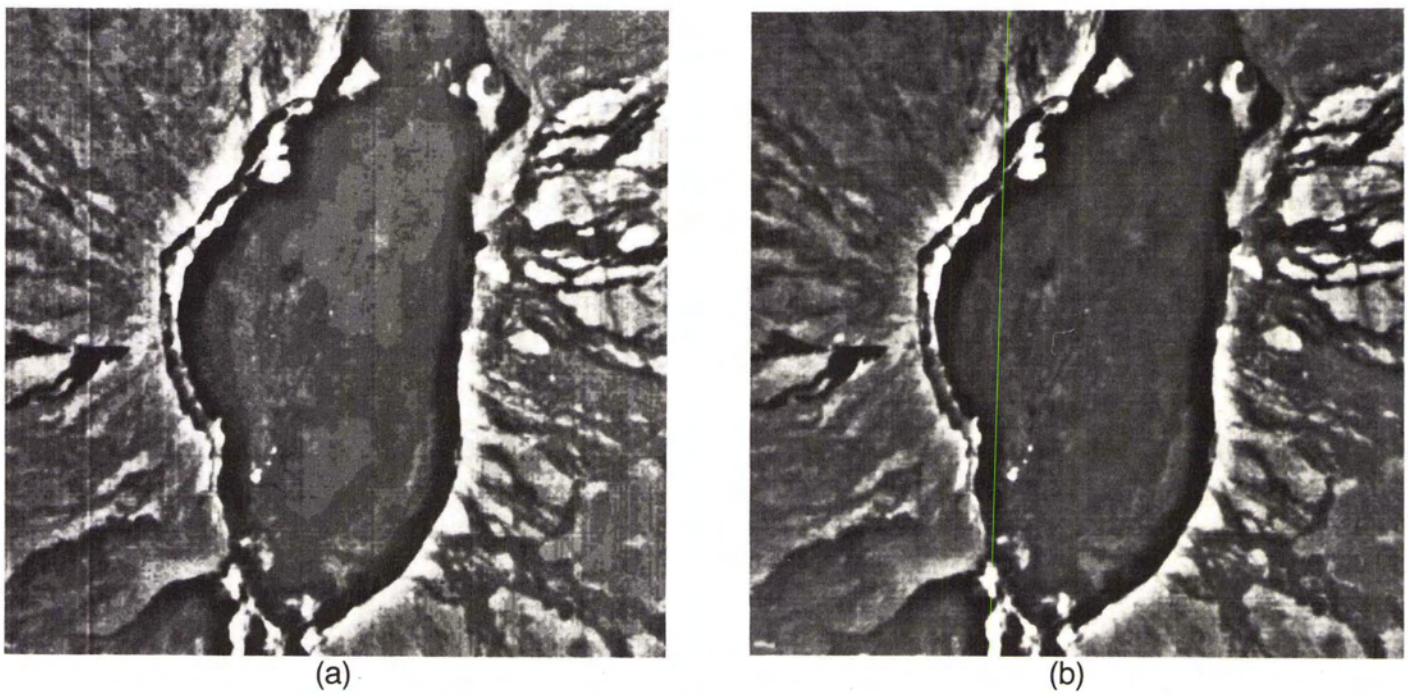

FIG. 3. (a) and (b) show the results of applying a 21 by 21 high-pass filter (HPF) to the normal- and high-gain XS2 images, respectively. These, like the 11 by 11 results, also show the quantizing/contouring effects. These data also had hard linear contrast stretches applied for visual analysis and display. SPOT image Copyright 1987 CNES.

8,8,7 during low sun elevation seasons and 7,7,6 during high sun elevation seasons.

What is needed in future systems (such as SPOT-3, Landsat-6, and EOS) is both a variable gain and a variable offset capability. By including variable offset, the radiance value that is mapped to zero DN can be changed according to the minimum reflectance value that is expected, or is of interest, in the area to be imaged. This would allow the reflectance range in both dark and bright regions to be maximized using predicted gain and offset settings. If only variable gain is available, bright re-

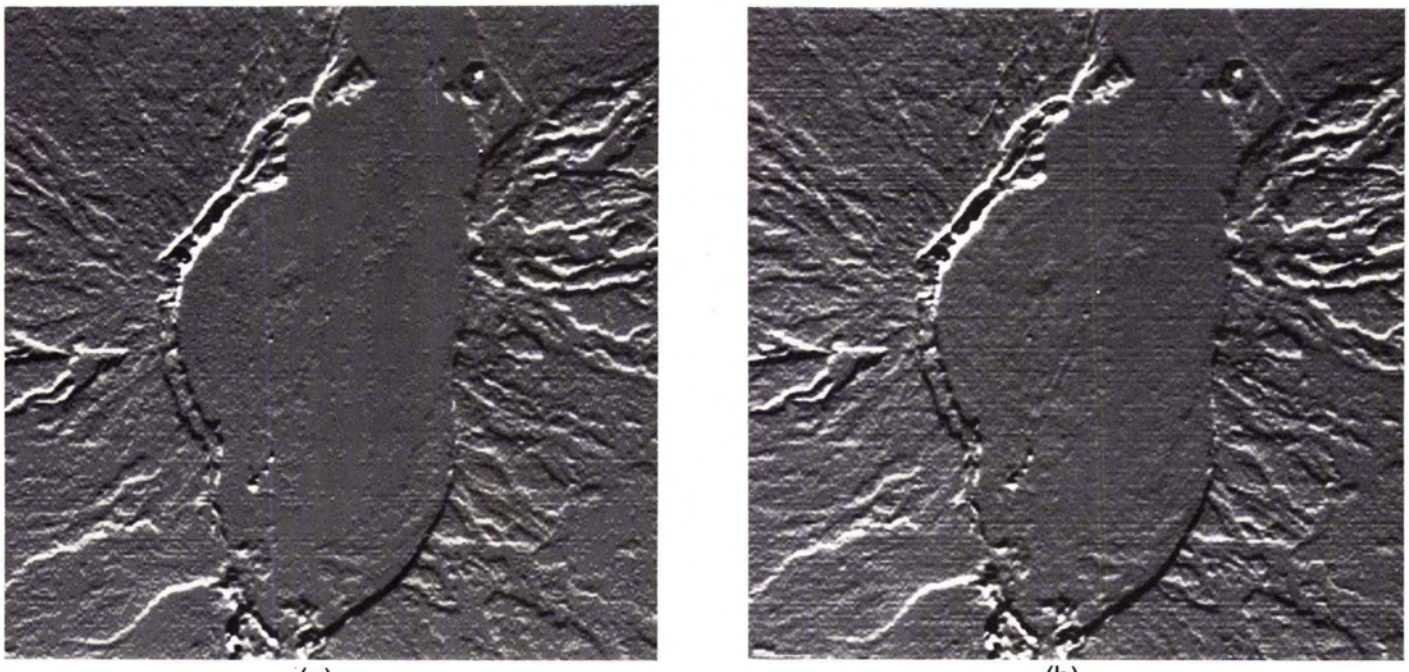

FIG. 4. (a) and (b) show the results of a vertical first difference, which approximates a first derivative, for the normal- and high-gain XS2 images, respectively. As predicted from the statistics shown in Table 1, the normal image is less busy and has more homogeneous areas, as is the case with the HPF results. These data also had hard linear contrast stretched applied for visual analysis and display. SPOT image Copyright 1987 CNES.

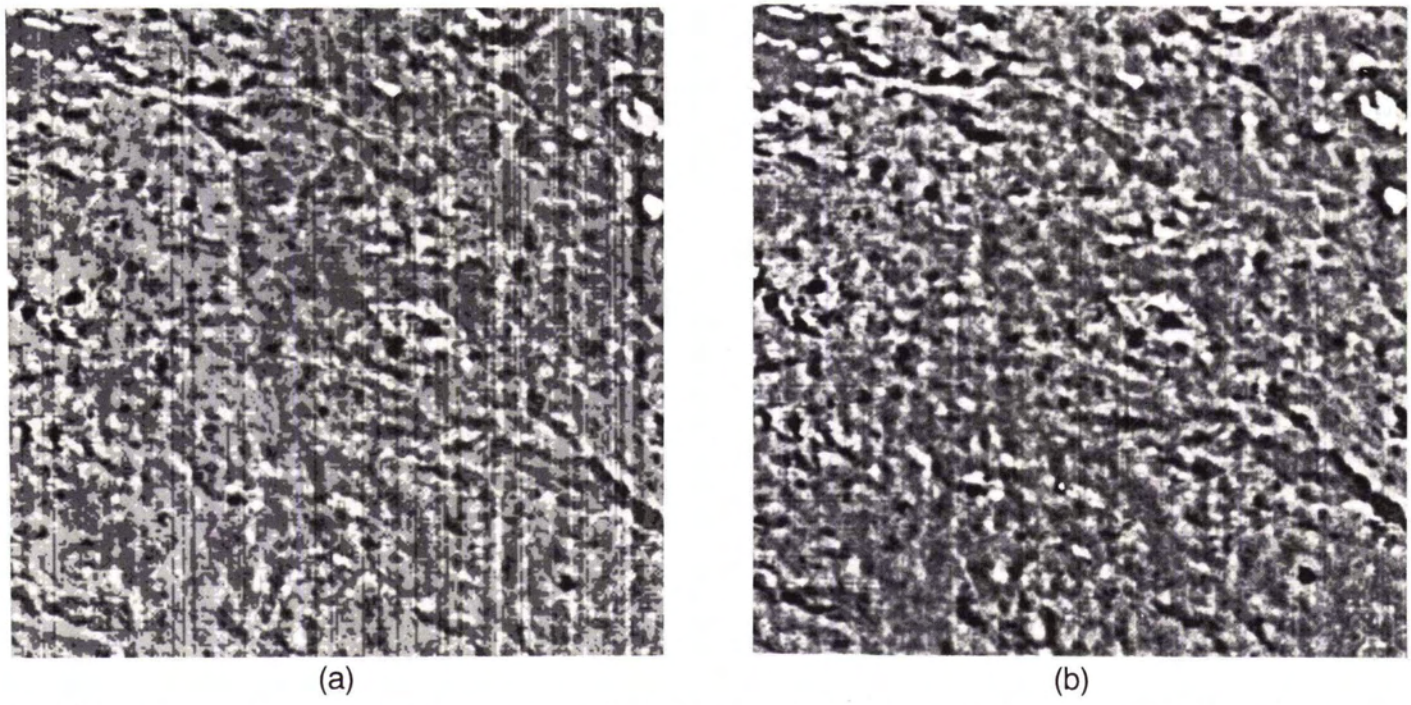

FIG. 5. (a) and (b) show the results of applying an 11 by 11 high-pass filter (HPF) to the normal- and high-gain XS3 images, respectively. The area is brighter than the dark Mauna Loa volcano; the DN values are in the mid-to-upper region of the entire image histogram (excluding clouds). Notice that the quantizing/contouring effect is also present in this area. The difference in the gain between the XS3 images is 2.2 as compared to 1.7 for the XS2 images. Also notice that the noise/stripping is greater for the normal image. This was generally the case for all three XS bands. SPOT image Copyright 1987 CNES.

gions will have the problem that a large percentage of the available DN range will be empty because it is "reserved" for reflectance levels much lower than those actually present in the area of interest.

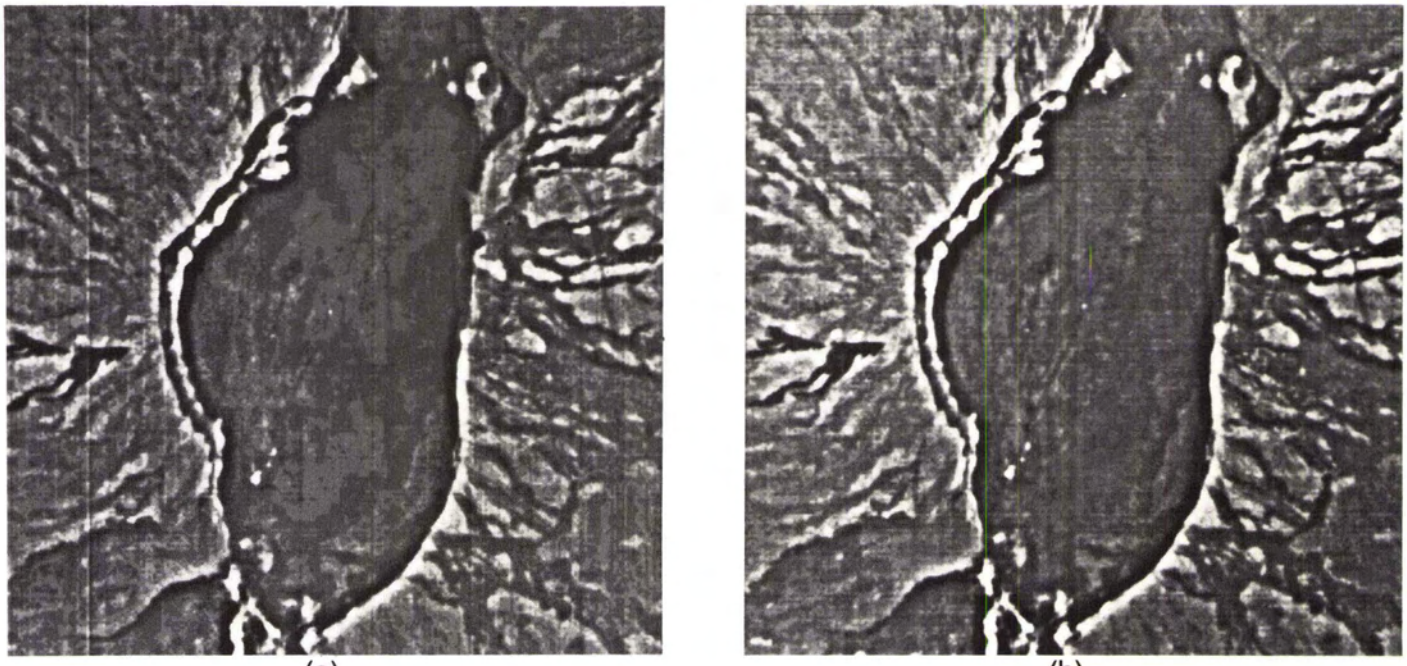

FIG. 2. (a) and (b) show the results of applying an 11 by 11 high-pass filter (HPF) to the normal- and high-gain XS2 images, respectively. The quantizing/contouring effects due to the smaller compressed DN range of the normal gain image (1.7 difference) can easily be seen, especially inside the Mauna Loa crater where the variation in reflectance is small. The HPF results had hard linear contrast stretches applied for visual analysis and display. SPOT image Copyright 1987 CNES.

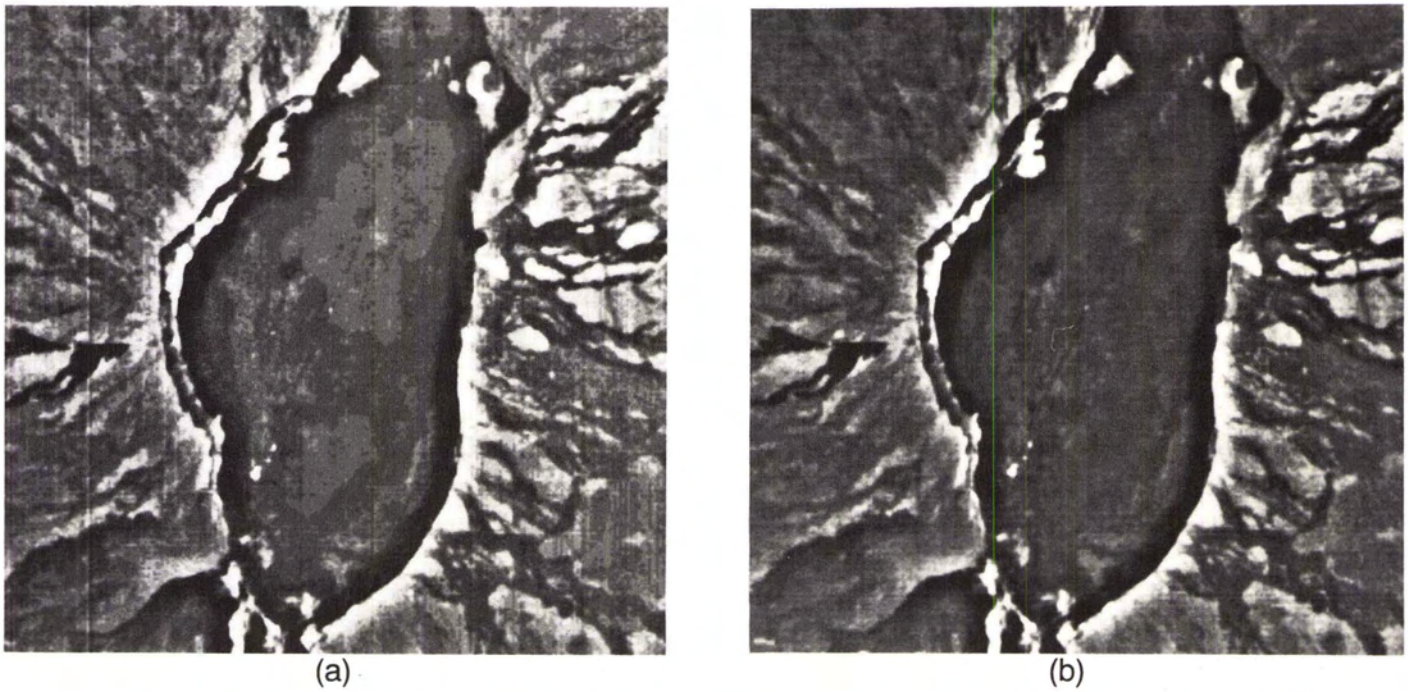

FIG. 3. (a) and (b) show the results of applying a 21 by 21 high-pass filter (HPF) to the normal- and high-gain XS2 images, respectively. These, like the 11 by 11 results, also show the quantizing/contouring effects. These data also had hard linear contrast stretches applied for visual analysis and display. SPOT image Copyright 1987 CNES.

8,8,7 during low sun elevation seasons and 7,7,6 during high sun elevation seasons.

What is needed in future systems (such as SPOT-3, Landsat-6, and EOS) is both a variable gain and a variable offset capability. By including variable offset, the radiance value that is mapped to zero DN can be changed according to the minimum reflectance value that is expected, or is of interest, in the area to be imaged. This would allow the reflectance range in both dark and bright regions to be maximized using predicted gain and offset settings. If only variable gain is available, bright re-

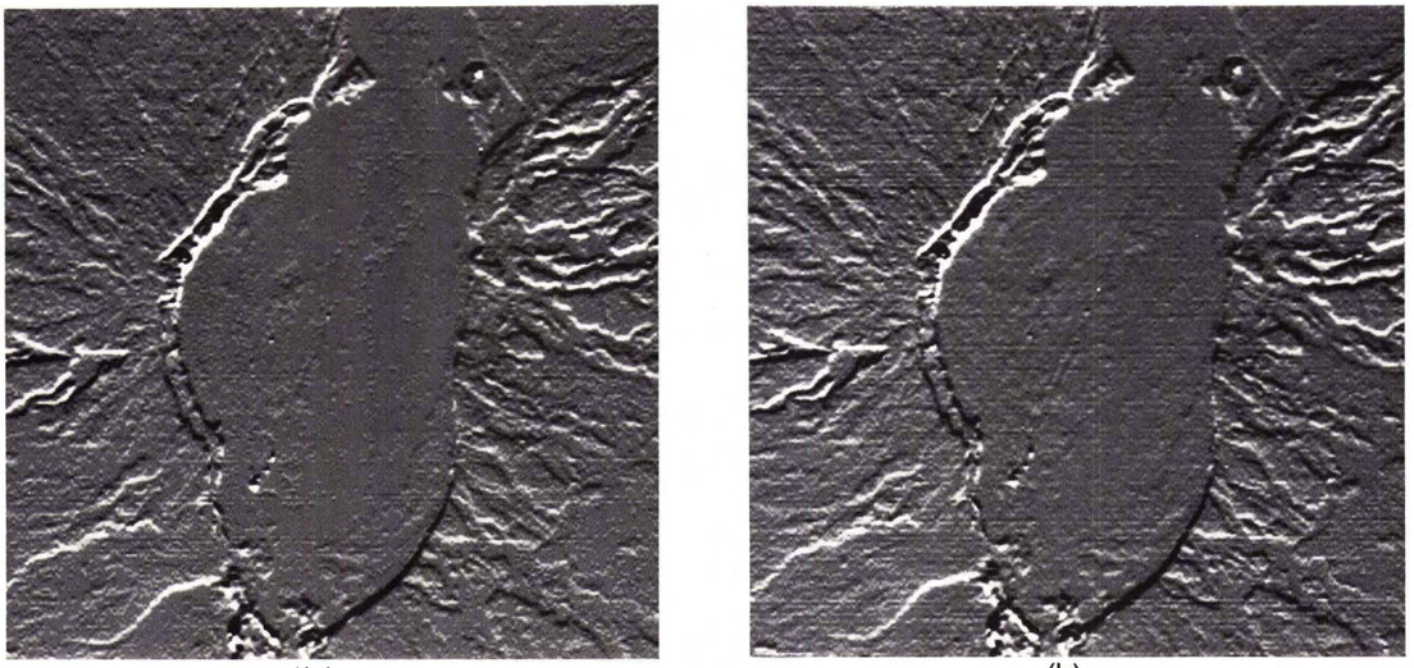

FIG. 4. (a) and (b) show the results of a vertical first difference, which approximates a first derivative, for the normal- and high-gain XS2 images, respectively. As predicted from the statistics shown in Table 1, the normal image is less busy and has more homogeneous areas, as is the case with the HPF results. These data also had hard linear contrast stretched applied for visual analysis and display. SPOT image Copyright 1987 CNES.

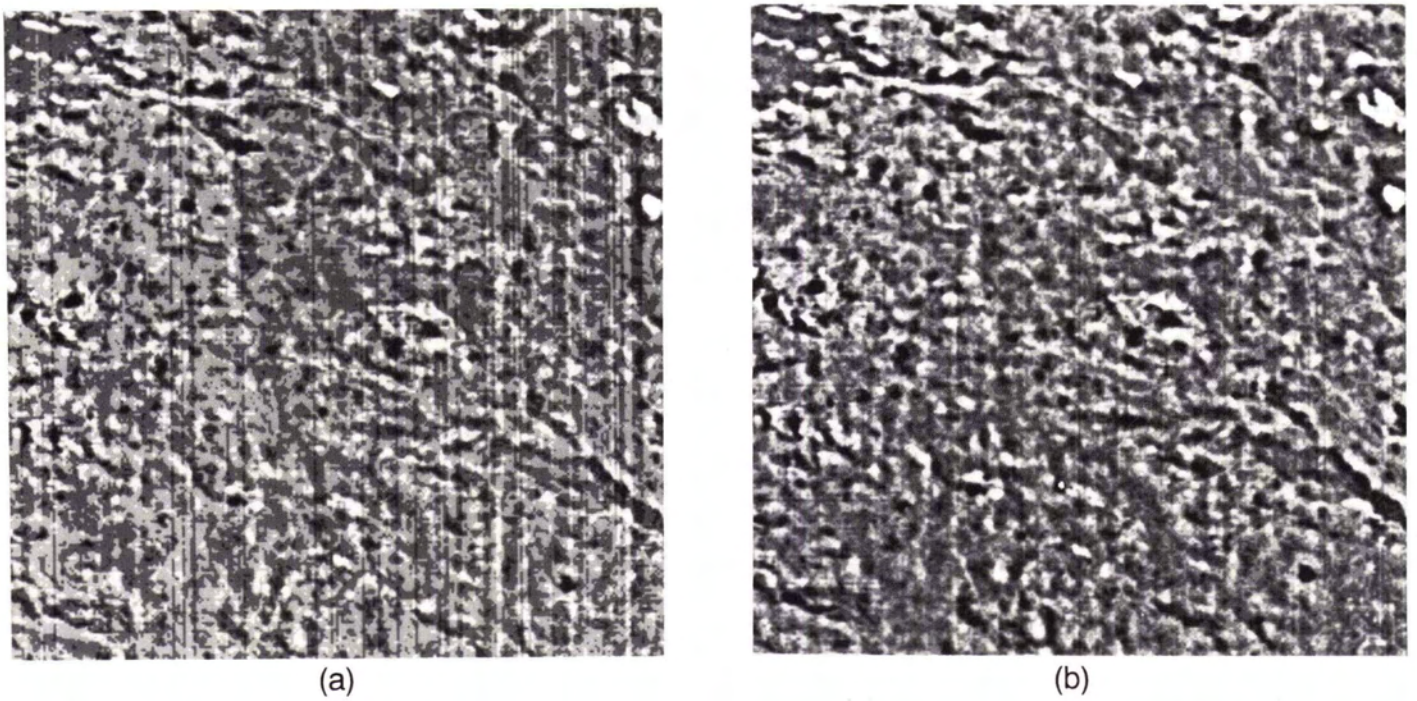

FIG. 5. (a) and (b) show the results of applying an 11 by 11 high-pass filter (HPF) to the normal- and high-gain XS3 images, respectively. The area is brighter than the dark Mauna Loa volcano; the DN values are in the mid-to-upper region of the entire image histogram (excluding clouds). Notice that the quantizing/contouring effect is also present in this area. The difference in the gain between the XS3 images is 2.2 as compared to 1.7 for the XS2 images. Also notice that the noise/stripping is greater for the normal image. This was generally the case for all three XS bands. SPOT image Copyright 1987 CNES.

gions will have the problem that a large percentage of the available DN range will be empty because it is "reserved" for reflectance levels much lower than those actually present in the area of interest.

ACKNOWLEDGMENTS

The author would like to thank Jo Ann Bowell of the USGS for her help in processing the image data. Special thanks go to both SPOT IMAGE and CNES (French Space Agency) for going into a special mode and collecting the SPOT normal- and high-again data simultaneously.

REFERENCES

Bengi, G., B. Boissin, and J. Perbos, 1985. SPOT image quality and post-launch assessment, *Journal of Advance Space Research*, Vol. 5, No. 5, pp. 51–60.

Chavez, P. S., Jr., 1988. An improved dark-object subtraction technique for atmospheric scattering correction of multispectral data, *Journal of Remote Sensing of Environment*, Vol. 24, No. 3, pp. 459–479.

Chavez, P. S., Jr., and B. Bauer, 1982. An automatic optimum kernel-size-selection technique for edge enhancement, *Journal of Remote Sensing of Environment*, Vol. 12, no. 38, pp. 23–38.

Chavez, P. S., Jr., and G. L. Berlin, 1984. Digital processing of SPOT simulator and Landsat TM data for the SP mountain region, Arizona; *SPOT Symposium, Scottsdale, Arizona, Proceedings*, pp. 56–66.

Chavez, P. S., Jr., G. L. Berlin, and A. V. Acosta, 1976. Computer processing of Landsat MSS digital data for linear enhancements, *Second W.T. Pecora Memorial Symposium, Sioux Falls, S.D., Proceedings*, pp. 235–250.

Chavez, P. S., Jr., Guptill, S. C., and Bowell, J., 1984. Image processing techniques for thematic mapper data: *50th Annual Conference of the American Society of Photogrammetry, Proceedings*, Vol. 2, Washington, D.C., pp. 728–743.

Courtois, M., 1984. SPOT system conception and program status: *SPOT Symposium, Scottsdale, Arizona*, pp. 8–18.

(Received 8 July 1988; accepted 14 September 1988; revised 10 October 1988)

BOOK REVIEW

Remote Sensing in Soil Science by M.A. Mulders. Elsevier. Amsterdam, Oxford, New York, Tokyo, 1987. 379 Pages. Hardcover.

THIS IS THE 15th Title in a "Developments in Soil Science" series by Elsevier Science Publishing Company. The book is divided into 14 chapters with subdivisions ranging from 7 to 13 sections per chapter. There are 5 color plates, 138 figures, and 32 tables.

As stated by the author, this book is written for professionals and students involved in the "geographical distribution of soils," hence encompassing the broad areas of soil science, geography, geology, hydrology, ecology, and agriculture. The book presents a comprehensive analysis of the state of remote sensing for soil mapping and survey applications. In fact, although an excellent soils and remote sensing book has been written, a more just title to this book might be remote sensing in soil survey. In the introductory chapter (Chapter 1), the author lays down the framework for the difficult task of bringing together the fields of remote sensing and soil science, with soil science defined as the mapping of soil bodies and the study of their dynamical aspects. For efficient utilization of remote sensing techniques in soil science, one needs a working knowledge of the physical interaction of electromagnetic radiation with the soil surface as well as knowledge of the physiographic and morphogenetic aspects of the landscape surface.

Chapter 2 deals with the physical concepts of electromagnetic radiation, including the basic radiation laws and the transmission of energy through the atmosphere. A very effective approach is taken in relating the microscopic interactions of energy with matter (vibrational, electronic, etc.) to the macroscopic signals of reflection, diffraction, and refraction. Thus, we are shown how surface absorption phenomena combine with surface roughness to produce surface and body "color" components to reflected energy. Energy balance and thermal properties are also covered in this chapter.

In Chapter 3, the interactions of electromagnetic radiation with minerals, leaves, soil materials, and plants are presented from a laboratory measurements perspective. The author is careful in building from the reflectance properties of the individual minerals and organic constituents to that of the soil material "assemblage." The same is done in differentiating leaves from entire plants; however, the assemblage of soil and vegetation, characteristic of incomplete canopies, is not covered. This chapter also includes a fair amount of directional reflectance and polarization data for soils and vegetated surfaces. Chapter 4 concerns the detection of electromagnetic radiation from the human vision system to the photographic and non-photographic techniques. An interesting and comprehensive treatment of color theory is included in this chapter.

The information extraction and image processing chapter (Chapter 5) is a relatively short chapter devoted to both photographic images and digital image data. Most of the information extraction techniques are statistical, involving automated classification, feature plane analysis, and principal component analysis. There is little attention to the extraction of physical parameters so well covered in the laboratory data from Chapter 2. There is some discussion of data structures but no mention of the "soil line" or "soil plane" concepts representative of primary soil data structures. Ratios and change detection methodologies were mentioned but not elaborated upon. Various image processing techniques such as edge enhancement and the use of low and high pass filters could also have been considered as they have been successfully used in geologic remote sensing.

Chapters 6 and 7 deal with basic image characteristics and aerial photography such as resolution, scale, tone, texture, patterns, contrasts, and colors. The general aspects of aerial photography and stereoscopy are covered with some discussion on the procedures for aerial surveying of land surfaces. Deciphering the maximum amount of land surface physiographic information using basic and inferred aspects for mapping is highlighted in Chapter 8. Although this is a very useful chapter, it does not go beyond the traditional realm of photointerpretation. Most of the discussion centers on what can be "seen" in images, leaving out the physico-chemical aspects of radiation interaction with the land.

In Chapter 9 we are shown how to make best use of airphotos for soil mapping and land evaluation purposes. Two examples of airphoto-interpretation over Surinam and Kenya are given and compliment the text material quite well. Airborne line scanning (Chapter 10) is treated separately from space-borne scanning (Chapter 11) due to the differences in platform height and hence resolutions. Besides a section on the various types of line scanners, there is some discussion on extracting basic soil prop-